Supporting Information for

Alkalinity and carbon production in coastal aquifers and their discharge into the coastal ocean

This PDF file includes:

Supporting S1 to S5
Figures S1 to S3
Tables S1 to S2
SI References

S.1. Methodology

We used 58 articles (Table S.1) to establish a dataset to characterize the total alkalinity (TA) and dissolved inorganic carbon (DIC) fluxes of fresh and saline coastal aquifers into the ocean. Since a few (8) articles contained data on both TA and DIC, we calculated DIC from the TA, pH, and major ions composition using the PHREEQC software (v. 3, 1). In all cases, concentrations are in $\mathrm{mol} \cdot \mathrm{kg_{H_2O}}^{-1}$ unless otherwise noted. The DIC is defined as the sum of all dissolved inorganic carbon species concentration in the water:

$$[\mathrm{DIC}] = [\mathrm{H_2CO_3^*}] + [\mathrm{HCO_3^-}] + [\mathrm{CO_3^{2-}}] \quad (1)$$

When $[H_2CO_3^*]$ is the total dissolved CO_2: $[H_2CO_3^*] = [CO_2(aq)] + [H_2CO_3]$.
The operational definition of total alkalinity (TA) is the equivalent sum of the titratable bases with strong acid, thus representing the aqueous system's neutralizing capacity. If the aquatic system is composed only of the weak bases of CO_2 and water, the carbonate alkalinity (CA) equation is:

$$[CA] = [\mathrm{HCO_3^-}] + 2[\mathrm{CO_3^{2-}}] + [\mathrm{OH^-}] - [\mathrm{H^+}] \quad (2)$$

The TA equation must include other proton acceptors if the aquatic system contains weak bases (or acids) besides CO_2. Acid-base systems other than aqueous carbonate are often neglected in natural waters, but they might be included in distinct cases (2):

$$[TA] = [\mathrm{HCO_3^-}] + 2[\mathrm{CO_3^{2-}}] + [\mathrm{NH_3}] + [\mathrm{HS^-}] + 2[\mathrm{S^{2-}}] + [\mathrm{H_3SiO_4^-}] + [\mathrm{H_2SiO_4^{2-}}] + [\mathrm{B(OH)_4^-}] + [\mathrm{Org^-}] + [\mathrm{HPO_4^{2-}}] + 2[\mathrm{PO_4^{3-}}] - [\mathrm{H_3PO_4}] + [\mathrm{OH^-}] - [\mathrm{H^+}] \quad (3)$$

In natural waters and groundwaters, the non-carbon species in the TA composition are usually negligible, so we can assume that most of it is carbonate; thus, TA equals CA. The TA term is used throughout our paper since there are occasional high sulfide concentrations or other species, as well as what is measured in the lab corresponds to TA. The relation between TA and DIC is given by[2]:

$$[TA] = [\mathrm{DIC}](\alpha_1 + 2\alpha_2) + [\mathrm{OH^-}] - [\mathrm{H^+}] \quad (4)$$

When: $\alpha_1 = \left(\frac{[H^+]}{K_1} + 1 + \frac{K_2}{[H^+]}\right)^{-1}$ and $\alpha_2 = \left(\frac{[H^+]^2}{K_1 K_2} + \frac{[H^+]}{K_2} + 1\right)^{-1}$. K_1 and K_2 are the equilibrium constants, which are known from the direct experimental determination of specific temperature and ionic strength (salinity). $[\mathrm{OH^-}]$ concentration can be calculated from $\mathrm{K_W} = [\mathrm{OH^-}][\mathrm{H^+}]$, $\mathrm{K_W}$ is the equilibrium constant for the self-ionization of water. $[\mathrm{H^+}]$ concentration is known from the relation $[\mathrm{H^+}] = 10^{-\mathrm{pH}}$. Therefore, for any pair of TA, pH, and DIC together with the ion composition (salinity) at 25°C PHREEQC can calculate the equilibrium constant and the species of the carbonate system and the unknown parameter (TA, pH, or DIC), in our case the DIC.

The DIC can be expressed as a function of P_{co_2}, thus it is possible to calculate it by the solution's TA and pH (2):

$$[TA] = \frac{K_H P_{co_2}}{\alpha_0}(\alpha_1 + 2\alpha_2) + K_{w/}[H^+] - [H^+] \quad (5)$$

where $\alpha_0 = \left(1 + \frac{K_1}{[H^+]} + \frac{K_1 K_2}{H^2}\right)^{-1}$ and K_H are Henry's law constant, the distribution coefficient in equilibrium between the liquid and gaseous phases of CO_2. For the calculation of the partial pressure equivalent lines of CO_2, we used PHREEQC software, where, for each line, we assumed a range of possible DIC and calculated the TA for the average groundwater composition at a given salinity (fresh, brackish, saline) and constant P_{co_2}.

Water measurements were divided into three categories based on chlorine concentration or salinity level: fresh, brackish, and saline. According to the description of the aquifer rock in each article (Table S1), we divided the data into four types of rock: carbonate, alluvium, sand, and basalt; however, there were very few measurements for basalts, so we also included one non-coastal aquifer to compare the effects of the rock on the carbon system parameters. A DIC calculation using pH and TA (papers 1-27 in Table S1) also requires ion composition; to have only reliable results, we calculated the charge balance for each water sample and included only samples with a value below 6%.

S.2. DIC and TA enrichment/depletion calculation

To evaluate the enrichment/depletion of the TA or DIC in relation to conservative mixing between fresh groundwater and seawater, the difference between the measured component concentration ($[DIC]_{measured}$) to the theoretical value based on only conservative mixing ($[DIC]_{mix}$) was calculated:

$$[\Delta DIC] = [DIC]_{measured} - [DIC]_{mix} \quad (6)$$

The theoretical mixing DIC concentration was calculated as a conservative mixing between two endmembers:

$$[DIC]_{mix} = f_{seawater} \cdot [DIC]_{seawater} + (1 - f_{seawater}) \cdot [DIC]_{freshwater} \quad (7)$$

The value was only calculated for water samples included in the database of the paper's seawater composition ($[DIC]_{seawater}$) , while for fresh endmembers, the freshest water sample was taken from that paper ($[DIC]_{freshwater}$). $f_{seawater}$ is the fraction of seawater, which is calculated from the measured chloride concentration in the groundwater sample in assuming this ion has a conservative behavior in this system:

$$f_{seawater} = \frac{[Cl^-]_{measured} - [Cl^-]_{freshwater}}{[Cl^-]_{seawater} - [Cl^-]_{freshwater}} \quad (8)$$

In Figure 2, the calculations [ΔDIC] and in the same way also [ΔTA] are shown. All the samples lying above the zero line are enriched with DIC and TA compared to conservative mixing of the two endmembers (fresh groundwater and seawater), and all the samples below this line are depleted. It is clear that most of the samples are on or above this line, and therefore, the aquifer can serve as a source for TA and DIC.

S.3. Determining the proportional contribution of each rock type to the total flow

The amount of freshwater discharge from each type of rock in the aquifer was calculated based on the work of Luijendijk et al., (2020), who calculated the SGD water discharge for coastal aquifers worldwide. In their work, they compared the geospatial database of drainage basins with the high-resolution geospatial database of surface lithology (GIS layer) described by Hartmann and Moosdorf (2012). In Table S2, we have narrowed down the 16 lithologies. Hartmann and Moosdorf (2012) divided the world map into five categories. The fresh SGD global calculation of Luijendijk et al. (2020) is based on parameter sensitivity analysis conducted numerically and upscaling the sensitivity analysis results to a global scale by calculating bilinear interpolations with global parameter databases. In their sensitivity analysis, they also calculated the saline SGD; however, contrary to the fresh SGD, they did not upscale the saline SGD to the global scale. We bridged this gap and calculated the saline SGD fluxes in all the coastal aquifers from their results in the same way. These simulations were done in a homogenous aquifer; however, Michael et al., (2016) reported that sediment heterogeneity increases the density-driven saline SGD flux by 20-100 times compared with that of homogenous models. Since Luijendijk et al. (2020) made the sensitivity analysis by a homogeneous model, we corrected the fluxes by a conservative factor of 20-100. The corrected total density-driven discharge is 400-2000 $km^3\ y^{-1}$. The density-driven saline SGD fluxes in all aquifers are detailed in Table 1. Using the same GIS database lithological division, we could divide the relative flow from each rock type for fresh and saline water using Hartmann & Moosdorf's (2012) detailed division (Fig. S1 A, B) and the reduction classification we used for this study (Fig. S1 C, D).

S.4. Using the database's rock type descriptions to calculate DIC and alkalinity SGD fluxes

We calculate the TA and DIC fluxes ($Tmol \cdot y^{-1}$) by the equation:

$$F_{fSGD,i} = [C]_i \times Q_i \quad (9)$$

When the freshwater flux ($F_{fSGD,i}$) was calculated for TA or DIC for each component i, the rock type in Table S2. [C] is the represented concentration of TA or DIC and $Q(km^3 \cdot$

y^{-1}) is the SGD water discharged for component i. Since in the saline flux, the groundwater contributes only the TA and DIC enrichment in relation to the seawater recharge to the aquifer, we used this equation:

$$F_{sSGD,i} = [\Delta C]_i \times Q_i \quad (10)$$

Also here the saline water flux ($F_{sSGD,i}$) was calculated for TA or DIC for each component i. $[\Delta C]_i$ is the enrichment factor of the circulated seawater concentration of TA or DIC as was calculated in Eq. 6.

S.5. Using the database's rock type descriptions to calculate DIC and alkalinity SGD fluxes

To investigate the characteristics of DIC and TA, we conducted data processing and statistical analyses on groundwater data. To understand the distribution of the combined datasets, we calculated the 20th, 50th, and 80th percentiles for both DIC and TA. We refined our datasets by retaining only data points between the 20th and 80th percentiles. This filtered dataset was used for subsequent analyses to reduce the influence of outliers. For each case, we computed the mean and standard deviation, which were used for flux evaluations in Table 1. These descriptive statistics helped us understand data variability and estimate errors. Fig. S2 shows the distributions of DIC and TA in freshwater samples for four rock-type aquifers (Sand, Alluvium, Carbonate, and Basalt) (upper plot) and saline water samples for short and long circulation from the shoreline (lower plot). The box plot's lower quartile is set to 0.20, and the upper quartile to 0.80. The mean (shown as a star) is generally higher than the median because the dataset contains many high outliers. Since we consider these outliers, we filtered them out before further analysis. Fig. S3 displays histograms of the filtered DIC and TA datasets in freshwater (upper plots) and saline water (lower plots) samples from the different aquifers. The median values and standard deviations are annotated on each subplot. The histograms show the concentration distributions of DIC and TA across the aquifer types. Comparing these histograms reveals differences in DIC and TA distributions among the aquifers, providing insights into their geochemical characteristics. Overall, these histograms deliver a comprehensive visual overview of the DIC and TA distributions across various aquifer types, aiding in comparative analysis and interpretation of the geochemical data.

According to these analyses, we calculated the flux by multiplying the corrected median by the discharge for each water source and rock type (from Fig. S1). The calculated fluxes and their sums and errors (based on the standard deviation) are summarized in Table 1.

146 **Table S1. Data source for the DIC – Alkalinity database from coastal aquifers around the world**

	Reference	Paper Name	Location	# of samples	Aquifer rock type	Salinity group	Rock type description	Sampling source	Distance from the shore
1	Magaritz and Luzier, 1985	Water-rock interactions and seawater-freshwater mixing effects in the coastal dunes aquifer, Coos Bay, Oregon	Coos Bay, Oregon, West Coast, USA	18	Sand	Fresh to saline	Shell-rich, gray marine sand (Pleistocene-Holocene), permeable dune sand.	Boreholes	0–500 m (shoreline to inland wells)
2	Chapelle et al., 1987	Bacteria in deep coastal plain sediments of Maryland: A possible source of CO_2 to groundwater	Maryland, USA	8	Sand	Fresh water	Sand formation	Boreholes	Inland from the immediate coastal mixing zones with seawater
3	Price and Herman, 1991	Geochemical investigation of salt-water intrusion into a coastal carbonate aquifer: Mallorca, Spain	Mallorca, Mediterranean Sea, Spain	19	Carbonate	from 10% to 90% sea water≤ *Included in saline SGD fluxes*	Limestone: The Camp de Tir site: eolian and beach calcarenite bedrock, highly porous. The Serra Nova site: bedrock covered by a thin layer of calcareous sand.	Boreholes	25m, 110m and 300m from the shore
4	Wicks et al., 1995	Water-rock interactions in a modern coastal mixing zone	West-central Florida, USA	62	Carbonate	Fresh and brackish *Included in saline SGD fluxes*	Eocene–Oligocene limestone and dolomite. The upper Floridan aquifer system consists of the Suwannee Limestone (Oligocene), the Ocala Limestone (late Eocene), and the Avon Park Formation (middle Eocene).	Boreholes	3.5 km from the shore
5	Wicks and Herman, 1996	Regional hydrogeochemistry of a modern coastal mixing zone	West-central Florida, USA	12	Carbonate	Fresh and brackish	Limestone and dolomite	Boreholes	0-9.5 km from the shore
6	Barker et al., 1998	Processes affecting groundwater chemistry in a zone of saline intrusion into an urban sandstone aquifer	Liverpool and the Mersey Estuary, England	14	Sand	Fresh to saline	Sandstone. The sandstones are sublitharenites and quartz arenites and their mineralogy is typically quartz (50-70%), with feldspar (5-15%), lithic clasts (3-8%) and carbonate clasts and cement (0-20%). Some beds are very micaceous and authigenic clays such as illite, smectite, and kaolinite are common.	Estuary, river, seawater, tunnel outflows, groundwater inflow, pumping station sump	550 m to 1175 m relative to estuary shoreline
7	Mahlknecht et al., 2004	Groundwater chemistry and mass transfers in the Independence aquifer,	Meseta Central, Central Mexico *Not a coastal aquifer*	7	Basalt	Freshwater	Basalt and alluvium Mainly of mafic rocks (basaltic lava flow, rhyolitic rocks). Lacustrine deposits of sands,	Boreholes	Inland, intermountain, sedimentary Independence Basin in central Mexico

	Reference	Paper Name	Location	# of samples	Aquifer rock type	Salinity group	Rock type description	Sampling source	Distance from the shore
		central Mexico, by using multivariate statistics and mass-balance models					interstratified by gravels and clay, and on occasion by sandstone and conglomerate.		
8	Andersen et al., 2005	Geochemical processes and solute transport at the seawater/freshwater interface of a sandy aquifer	Skansehage peninsula, Isefjord, northern part of Zealand, Denmark	4	Sand	Fresh to saline	Coastal siliclastic aquifer containing minor amounts of calcite.	Piezometers	A 120 m transect extending from the coastline and landward
9	Charideh and Rahman, 2007	Environmental isotopic and hydrochemical study of water in the karst aquifer and submarine springs of the Syrian coast	Syria	16	Carbonate	mixing zone between fresh groundwater and seawater.	Karstified limestone and dolomite aquifer systems.	Springs and boreholes	wells are located along the coastal line. Submarine springs discharge at various depths below sea level.
10	Bouchaou et al., 2008	Application of multiple isotopic and geochemical tracers for investigation of recharge, salinization, and residence time of water in the Souss–Massa aquifer, southwest of Morocco	Souss–Massa aquifer, southwest of Morocco	85	Alluvium	Coastal: modern seawater intrusion; Inland: fresh to fossil seawater influence	Plio-Quaternary sediments (sands, gravels, and lacustrine limestone), some layers contain evaporated minerals (gypsum in Jurassic and Cretaceous, and halite in Triassic formations).	Springs and boreholes	0 m (coast) to far inland (up to High Atlas region). Groundwater from coastal plains, inland plains, and mountain recharge zones
11	de Montety et al., 2008	Origin of groundwater salinity and hydrogeochemical processes in a confined coastal aquifer: Case of the Rhône delta (Southern France)	Rhône Delta, Southern France	8	Alluvium	Freshwater mixtures with seawater	Quaternary deposits of the delta. Two levels of deposits are distinguished within the gravels. The first deposit (Lower Pleistocene) is mainly made of highly altered gravels of quartzite and limestone with a yellow matrix of sand and sometimes marl or clay (mainly montmorillonite). In the second deposit (Upper Pleistocene), the gravels are not altered and are more diversified (including green rocks, variolites, and crystalline rocks).	Piezometers	between 8 km and 20 km from the coast
12	Gattacceca et al., 2009	Isotopic and geochemical characterization of salinization in the shallow aquifers of a reclaimed subsiding zone: The southern	Southern Venice Lagoon coastland, Italy	12	Alluvium	Fresh to saline	A complex heterogeneous mixture of highly calcareous layers (sandy and silty–clayey) with local clay lenses and peat layers (Brambati	Boreholes	0–7 km (saline zone), 7–20 km inland (brackish zone)

	Reference	Paper Name	Location	# of samples	Aquifer rock type	Salinity group	Rock type description	Sampling source	Distance from the shore
		Venice Lagoon coastland							
13	Chae et al., 2012	Seawater–freshwater mixing and resulting calcite dissolution: an example from a coastal alluvial aquifer in eastern South Korea	Okgye area, Eastern Coast, South Korea	3	Alluvium	Fresh water - seawater mixtures	Alluvial groundwater in a limestone-rich coastal area	Boreholes	One site is located within 1 km of the coastline, and the other is located approximately 2.5 km away.
14	Vandenbohe de and Lebbe, 2012	Groundwater chemistry patterns in the phreatic aquifer of the central Belgian coastal plain	The central Belgian coastal plain, North Sea coast, Belgium	18	Sand	Fresh water - seawater mixtures	Fluvial and marine deposits (mainly coarse sand)	Boreholes	Between few meters up to 2.5 km from the shore.
15	Ahmed et al., 2013	Factors controlling mechanisms of groundwater salinization and hydrogeochemical processes in the Quaternary aquifer of the Eastern Nile Delta, Egypt	Eastern Nile Delta, Egypt	61	Alluvium	Fresh to brackish	Deltaic deposits: Nile silt, old deltaic sands, and gravels which are underlain by fluvio-marine deposits	8 canals, 12 drains, and 41 boreholes	No specific distance information. A range of distances from the shore, from near 0 m at the northern coast to potentially over 100 km inland.
16	Vinson et al., 2013	Occurrence and mobilization of radium in fresh to saline coastal groundwater inferred from geochemical and isotopic tracers (Sr, S, O, H, Ra, Rn)	Agadir, southwestern Morocco	17	Alluvium	Fresh to brackish	The primary aquifer consists of overlying Pliocene to Pleistocene transgressive deposits, up to 100 m of marine clay, sand, gravel, and limestone, overlain by conglomerate, sandy limestone, and shelly sandstone, with sandstone and conglomerate being important water-yielding units.	Boreholes	From few meters up to 5 km fron the seashore.
16	Vinson et al., 2013	Occurrence and mobilization of radium in fresh to saline coastal groundwater inferred from geochemical and isotopic tracers (Sr, S, O, H, Ra, Rn)	Confined Cretaceous (Cape Fear) and Pliocene (Yorktown) aquifers of the Atlantic Coastal Plain, North Carolina, USA	22	Alluvium	Fresh to brackish	Cape Fear formation is interpreted as deltaic deposits including offshore components. The Yorktown aquifer is composed of marine sand and clay containing abundant shell material and is locally phosphatic	Boreholes	In the Yorktown aquifer very close to the shore, and in the Cape Fear aquifers between 10 and 50 kilometers, approximately.
17	Zhang et al., 2015	Geochemical and isotopic data for restricting seawater intrusion and groundwater circulation in a series	Leizhou peninsular, South China Sea	16	Sand and volcanic rocks	Fresh to brackish	Sandy soil and pore fractured volcanic compose the main aquifers, whereas impermeable clay layers act as aquicludes	Borehols and ponds	From near shore up to 10 km.

	Reference	Paper Name	Location	# of samples	Aquifer rock type	Salinity group	Rock type description	Sampling source	Distance from the shore
		of typical volcanic islands in the South China Sea							
18	Díaz-Puga et al., 2016	Groundwater flow and residence time in a karst aquifer using ion and isotope characterization	Sierra de Gador, SE Spain	64	Carbonate	Fresh	Karst carbonate massif: carbonate rocks (dolostone and limestone) with interlayers of more soluble mineral phases (e.g. anhydrite, gypsum, and minor halite and fluorite)	Springs and wells	From near shore up to 20 km.
19	Han et al., 2016	Identification of anthropogenic and natural inputs of sulfate into a karstic coastal groundwater system in northeast China: evidence from major ions, $\delta^{13}C_{DIC}$ and $\delta^{34}S_{SO4}$	Daweijia area of Dalian, Bohai Sea coast, northeast China	10	Limestone and Alluvium	Brackish	The upper aquifer is composed of Quaternary sediments consisting of gravel, sand, and clay layers. The carbonate aquifers underlying the Quaternary deposits are mainly composed of limestone, with major karst development.	Boreholes	1-8 km from the shore.
20	Sajil Kumar, 2016	Deciphering the groundwater–saline water interaction in a complex coastal aquifer in South India using statistical and hydrochemical mixing models	Cuddalore district, Tamil Nadu, Southern India	11	Alluvium	Fresh	Fluvial fluvio-marine and marine facies: soil, fine to coarse-grained sands, silts, clays laterite, and lateritic gravels the semi-consolidated formations comprising silts, clay stones, calcareous sandstones, siliceous limestones, and algal limestones.	Boreholes	From near shore up to 40 km.
21	Santoni et al., 2016	Residence time, mineralization processes, and groundwater origin within a carbonate coastal aquifer with a thick unsaturated zone	Bonifacio plateau, southeast Corsica, western Mediterranean, France	15	Carbonate	Fresh	The base of fluvial detrital series (weathered granites with a carbonated fraction, ignimbritic tufa) A second set composed of carbonate marine sediments (shelly litharenites, sandy silt, and coralline-rich calcarenites). At the base, are calcareous sandstones and sandy calcarenites. Above, coralline sandstones with limestone cement and coralline sandy calcarenites. Many lenses filled with gravel material are present. Well-cemented limestone completes the series.	Boreholes	From several meters up to about 3 km from the shore.
22	Carreira et al., 2018	Tracing salinization processes in coastal aquifers using an isotopic and	Essaouira, Atlantic Ocean coast, western Morocco	10	Sand	Fresh to brackish	Detrital deposits (sandstones, conglomerates, and sands) and calco-dolomitic layers	Springs, boreholes	From few km uo to 50 km.

	Reference	Paper Name	Location	# of samples	Aquifer rock type	Salinity group	Rock type description	Sampling source	Distance from the shore
		geochemical approach: comparative studies in western Morocco and southwest Portugal							
22	Carreira et al., 2018	Tracing salinization processes in coastal aquifers using an isotopic and geochemical approach: comparative studies in western Morocco and southwest Portugal	Lower Tagus–Sado sedimentary, southwest Portugal	35	Alluvium	Fresh to brackish	Alluvial formations, sand and clay layers, sandstones and limestones	Springs, boreholes	From close to the shore up to few tens of km.
23	Han and Currell, 2018	Delineating multiple salinization processes in a coastal plain aquifer, northern China: hydrochemical and isotopic evidence	Yang–Dai coastal river plain, Qinhuangdao City, Hebei province, Northern China	34	Sand	Fresh to saline	Medium sand, coarse sand, and gravel layers	Production wells	Fron near shore up to 12 km.
24	Vallejos et al., 2018	Influence of the paleogeographic evolution on the groundwater salinity in a coastal aquifer. Cabo de Gata aquifer, SE Spain	Cabo de Gata, south-east of the Iberian Peninsula, Spain	22	Sand	Brackish, saline and hypersaline	Plio-Pleistocene conglomerate and sandstone with a mean thickness of 80 m. The top of the formation comprises cemented conglomerate and beneath these is a thick layer of sandstone. Underlying this are intercalations of conglomerate and sand.	Boreholes	The nine boreholes, situated between 350 and 650 m from the coast.
25	Mohanty and Rao, 2019	Hydrogeochemical, seawater intrusion, and oxygen isotope studies on a coastal region in the Puri District of Odisha, India	Puri District of Odisha, India	25	Alluvium	Fresh to brackish	Fluvial-deltaic sediments - sand, silt, clay, gravel, pebbles. The unconfined aquifer consists of alluvium, clay, and granular material and the deeper aquifer consists of sands, and pebbles with intercalated clay bands.	Boreholes	From 4 to 12 km from the Bay of Bangal coast
26	Monnin et al., 2019	Freshening of a Coastal Karst Aquifer Revealed by the Temporal Changes in a Spring Water Composition (La Palme, Southern France)	La Palme, Mediterranean coast, Southern France	11	Carbonate	Brackish	Karstic aquifer, Jurassic-Lower Cretaceous limestone formations with a thickness of ~200	Springs	Approximately 3 km inland from the present-day shoreline
27	Naus et al., 2019	Groundwater salinity variation in Upazila Assasuni (southwestern Bangladesh), as	Upazila Assasuni, southwestern Bangladesh	108	Sand	Fresh to brackish	Sands with carbonates with small discontinuous organic-matter-rich clay layers	Boreholes	Within ~6.3 km coastal delta (exact shoreline distance not specified)

	Reference	Paper Name	Location	# of samples	Aquifer rock type	Salinity group	Rock type description	Sampling source	Distance from the shore
		steered by surface clay layer thickness, relative elevation, and present-day land use							
28	Yechieli et al., 2019	Recent seawater intrusion into deep aquifer determined by the radioactive noble-gas isotopes ^{81}Kr and ^{39}Ar	Yarkon–Taninim Basin, Eastern Mediterranean coast, Israel	6	Carbonate	Brackish to saline	Karstic limestones and dolomites with some marls and chalks	Boreholes	Between few km up to ~20 km
29	Houéménou et al., 2020	Degradation of groundwater quality in expanding cities in West Africa. A T case study of the unregulated shallow aquifer in Cotonou	Cotonou, Atlantic Ocean Benin, West Africa	43	Alluvium	Fresh	fine to medium sands (85.5%), silts (5.5%) and clays (9%)	Boreholes, piezometers	Between about 2.5 to 5 km from the ocean coast, some of the sampling points are adjacent to the lake shore.
30	Okuhata et al., 2020	Metal Mobilization As An Effect of Anthropogenic Contamination in Groundwater Aquifers in Tutuila, American Samoa	Tutuila, American Samoa, South Pacific	18	Basalt	Fresh	Pleistocene age complex of volcanic shields deeply eroded into a rugged, mountainous edifice, while Holocene age rejuvenated volcanic eruptions later built the relatively flat relatively flat Tafuna–Leone Plain on the shields' southwestern flank.	Boreholes, springs	The island features coastal springs along its shores, upland springs located up to 2 km from the shore, and boreholes situated up to 6 km away from the coasts.
31	Pain et al., 2020	Carbon and phosphorus processing in a carbonate karst aquifer and delivery to the coastal ocean	Puerto Morelos, Yucatan, Mexico	20	carbonate	Fresh to saline	karstic carbonate platform of Triassic to Holocene age.	Cenotes, springs, borehole	Inland cenotes were sampled approximately 21 km inland from the coast. The near-shore well was located approximately 100 m inland. The SGD springs are distributed along the shore.
32	Vallejos et al., 2020	Anthropic-induced salinization in a dolomite coastal aquifer. Hydrogeochemical processes	Balanegra, Mediterranean Sea, SE Spain	45	Carbonate	Fresh to brackish	Dolomite and dolomitic limestone	Boreholes	Coastline up to 10 km from the shore
33	Godfrey et al., 2021	$\delta^{13}C$ and ^{14}C activity of groundwater DOC and DIC in the volcanically active and arid Loa Basin of northern Chile	Río Loa Basin Northern Chile	9	Basalt and alluvial	Fresh to brackish	Fractured basaltic andesite lava, dacitic and rhyodacitic ignimbrite, or unconsolidated ash and volcanic debris flows. Stacked aquifers occur within	Boreholes, springs	100–200 km inland from Pacific Ocean

	Reference	Paper Name	Location	# of samples	Aquifer rock type	Salinity group	Rock type description	Sampling source	Distance from the shore
							palustrine-lacustrine limestone and conglomerate gravels.		
34	Zhang and Zhang, 2021	The hydrological connection between fresh submarine groundwater discharge and coastal groundwater: an isotopic and a decadal hydrochemistry approach in an alluvial fan, central Japan	Katakai alluvial fan, Sea of Japan, Japan	13	Alluvium	Freshwater	The alluvial fan consists of three layers: A. alluvium of gravel, sand, and clay. B. gravel, sand, and clay. C. sandstone and mudstone.	Boreholes, SGD flux chamber	The boeholes' locations are from near shore up to 5 km, SGD sites are located 150–200 m seaward from the coastline.
35	Sola and Vallejos, 2022	Long and short-term cation exchange linked to a negative hydraulic barrier in a coastal aquifer	The Andarax Delta Aquifer, SE Spain	47	Alluvium	Freshwater –seawater mixing	Conglomerate, sand, and thin silt levels.	Boreholes	Close to the shoreline up to 1 km.
36	Cai et al., 2003	The geochemistry of dissolved inorganic carbon in a surficial groundwater aquifer in North Inlet, South Carolina, and the Carbon fluxes to the coastal ocean	North Inlet, Georgetown County, South Carolina, USA	13	Sand	Fresh to brackish	Unconsolidated and semiconsolidated layers of sand and clay, and poorly indurated to very dense layers of limestone and dolomite.	Piezometer	The piezometer transects are from the shore line across the marsh swale up to 500 m.
37	Gramling et al., 2003	A carbon isotope method to quantify groundwater discharge at the land-sea interface	Cape Fear region of southeastern North Carolina, USA	19	Carbonate	Fresh to brackish	consisting primarily of shell limestone, dolomitic limestone, sandy limestone, and fine to medium sand	Boreholes	varying distances from the immediate shoreline up to 4 km.
38	Sivan et al., 2005	Geochemical evolution and timescale of seawater intrusion into the coastal aquifer of Israel	Poleg area , Netanya, Mediterranean coastal aquifer, Israel	19	Sand	Freshwater to saline *Included in saline SGD fluxes*	Interlayered sand, calcareous sandstone (Kurkar), red loam (Hamra) and marine clays of the Pleistocene age	Boreholes	70 m from the shoreline
39	Russak and Sivan, 2010	Hydrogeochemical tool to identify salinization or freshening of coastal aquifers determined from combined fieldwork, experiments, and modeling	Mediterranean coastal aquifer and the Poleg area, Israel	5	Sand	Btackish to saline	Calcareous sandstone (Kurkar), red loam (Hamra) and marine clays of the Pleistocene age	Boreholes	70 m from the shoreline
40	Bakari et al., 2012	Groundwater residence time and paleo recharge	Southeastern Tanzania	19	Alluvium	Fresh	limestone and conglomerates interbedded by sandy clays and	Boreholes	The shallow unconfined aquifer located less than 5 km from the Indian

	Reference	Paper Name	Location	# of samples	Aquifer rock type	Salinity group	Rock type description	Sampling source	Distance from the shore
		conditions in the deep confined aquifers of the coastal watershed, Southeast Tanzania					clayey sands with minor lenses of pure sand or clay		Ocean. The deep confined aquifer is recharged from inland areas, the sampling sies are located up to 20 km from the shore.
41	Liu et al., 2012	How significant is submarine groundwater discharge and its associated dissolved inorganic carbon in a river-dominated shelf system?	Huiyang District, northern South China Sea, China	13	Sand	Fresh to brackish	The aquifer in the littoral plain is a sandy lens up to 20 m thick,	Boreholes, springs	Close to the shoreline.
42	Liu et al., 2014	Effect of submarine groundwater discharge on the coastal ocean inorganic carbon cycle	Charlotte Harbor, FL, USA	44	Limestone	Fresh to brackish	Subtropicalcarbonate platforms often overlying karstic limestone comprised of abundant fossil mollusk and calcareous and coralline algae	Boreholes, piezometers	
43	Wang et al., 2014	Coastal Acidification Induced by Tidal-Driven Submarine Groundwater Discharge in a Coastal Coral Reef System	Sanya Bay, Hainan Island, northern South China Sea, China	13	Alluvium	Saline	Holocene deposits of coral debris, sand, and silt surround the coast,	Boreholes	~100 m away from the shore.
44	Lee and Kim, 2015	Dependence of coastal water pH increases on submarine groundwater discharge off a volcanic island	Hwasun Bay off the volcanic island of Jeju, Korea	11	Basalt	Brackish to saline	Basaltic rocks, along the coast sandy sediments that overlie the thick and highly permeable basaltic layer.	Boreholes, onboard a ship by use of a submersible pump	Seawater sampling stations were located inside the bay and outside the bay. The transect line for vertical distribution measurements extended from the shoreline to about 1.0 km offshore. Groundwater samples were collected along the shoreline.
45	Wang et al., 2015	Net subterranean estuarine export fluxes of dissolved inorganic C, N, P, Si, and total alkalinity into the Jiulong River estuary, China	Xiamen Bay, China	24	Alluvium	Fresh to brackish	sands, clayey silts, and silty clay	Boreholes	The wells were located within 2.2 km distance from the water channel.
46	Sadat-Noori et al., 2016	Groundwater Discharge as a Source of Dissolved Carbon and Greenhouse Gases	Hat Head, NSW, Australia	27	Sand	Fresh to saline	Sandy beach environment	Push point piezometer, boreholes	Shallow groundwater wells were dug adjacent to the estuary. Deep monitoring wells were

	Reference	Paper Name	Location	# of samples	Aquifer rock type	Salinity group	Rock type description	Sampling source	Distance from the shore
		in a Subtropical Estuary							located across the catchment up to 1200 m from the seashore.
47	Bryan et al., 2017	Carbon dynamics in a Late Quaternary-age coastal limestone aquifer system undergoing saltwater intrusion	Rottnest Island, south-west Western Australia	29	Carbonate	Fresh to saline	Limestone varies from strongly lithified to friable which contains various proportions of quartz sand, fine- to medium-grained shell fragments, and minor clayey lenses.	Boreholes	From few meter up to about 1 km from the shoreline.
48	Caschetto et al., 2017	Nitrogen and sulfur cycling in the saline coastal aquifer of Ferrara, Italy. A multi-isotope approach	Ferrara, Italy	22	Sand	Fresh to saline	Sandy units and shallow marine wedge deposits	Boreholes	Near shore up to 20 km from the shore.
49	Liu et al., 2017	Carbonate system biogeochemistry in a subterranean estuary – Waquoit Bay, USA	Waquoit Bay, Cape Cod, Massachusetts, USA	175	Sand	Freshwater -saltwater mixing *Included in saline SGD fluxes*	Coarse and fine sand as well as gravel.	Piezometer	Between 3.5 m inland and 3 m seaward.
50	Prouty et al., 2017	Vulnerability of Coral Reefs to Bioerosion From Land-BasedSources of Pollution	Maui, HI, USA	150	Carbonate	Brackish to saline	nearshore coral reef ecosystems	Piezometers	Seep sites up to 52 m offshore in the coral reef.
51	Bandara et al., 2018	Arsenic-rich shallow groundwater in sandy aquifer systems buffered by rising carbonate waters: A geochemical case study from Mannar Island, Sri Lanka	Mannar Island, Sri Lanka	35	Sand	Fresh	Sand dunes	Boreholes	From near shore up to 2 km from the sealine (in the middle of the island).
52	Meredith et al., 2018	Evolution of dissolved inorganic carbon in groundwater recharged by cyclones and groundwater age estimations using the ^{14}C statistical approach	Pardoo Ck, WA, Australia	23	Sand	Fresh	Wallal Sandstone is the main aquifer in the multilayered aquifer system of the West Canning Basin. Semi-confined artesian aquifer. It comprises sandstone with rare siltstones and gravel interbeds.	Boreholes	From near shore up to 30 km.
53	Murgulet et al., 2018	Temporal and spatial fluctuations of groundwater-derived alkalinity fluxes to a semiarid coastal embayment	Nueces Bay, TX, USA	35	Sand	Fresh to saline	High sand percentage: The north-bay region has sandier sediments with a lower clay content (~20%), compared to the West-bay and Mid-bay, ~35–50% clay. In the deeper layers consist of less permeable	Retract-a-tip sampler (porewater), boreholes	From near shore up to 30 km (for the deep wells).

	Reference	Paper Name	Location	# of samples	Aquifer rock type	Salinity group	Rock type description	Sampling source	Distance from the shore
							materials such as mud, clay, and silts saturated with high salt content water.		
54	Tan et al., 2018	Shelf-Scale Submarine Groundwater Discharge in the Northern South China Sea and East China Sea and its Geochemical Impacts	Pearl River, northern South and the East China Sea shelf, China	48	Alluvium	Fresh to saline	The surface sediments on the NSCS continental shelf show grain size gradations from gravel inshore to soil offshore. The region along the shoreline of the NSCS is composed of thick and widespread quaternary deposits, with terrigenous and biogenous detritus as the major components	Boreholes and PushPoint sampler	Along the shore and offshore.
55	Dai et al., 2021	Submarine Groundwater Discharge on the Western Shelf of the Northern South China Sea Influenced by the Pearl River Plume and Upwelling	Pearl River, western shelf of the Northern South China Sea, China	8	Sand	Saline	Sandy beach	Pushpoint sampler and a peristatic Pump.	Water samples were collected along nine cross-shelf transects, spanning from nearshore to offshore, up to 51 km offshore.
56	Kolker et al., 2021	An Initial Assessment of the Contribution of Fresh Submarine Ground Water Discharge to the Alkalinity Budget of the Mediterranean Sea	Shikmona shore, Haifa, Israel	27	Carbonate	Brackish	Mostly carbonate rocks of the Judea group such as limestone, chalk, and dolomite. The shore is fringed by Kurkar (sand and calcite cemented sandstone) abrasion platforms.	Springs	Shoreline
57	Liu et al., 2021	Inorganic carbon and alkalinity biogeochemistry and fluxes in an intertidal beach aquifer: Implications for ocean acidification	Tolo Harbor, Hong Kong	208	Sand	Fresh to saline	The sediments of the sandy beach can be classified as well sorted gravelly sand.	Piezometer and boreholes	The sampling points ranged from approximately 50 m landward to 50 m seaward of the mean tidal mark, with zones like the mangrove area located between 50 and 30 m and the high salinity zone spanning from 30 to 50 m.
58	Reithmaier et al., 2021	Rainfall drives rapid shifts in carbon and nutrient source-sink dynamics of an urbanized, mangrove-fringed estuary	Coffs Creek, east coast of New South Wales, Australia	12	Alluvium	Brackish to saline	Basalt-derived podzolic soils and unconsolidated sediments consisting of clay, silt, sand, and gravel deposits at the estuarine deltas	Boreholes	0–6.2 km along estuary (intertidal mangrove zone)

147

148 **Table S2. Rock type classifications**

This study aquifer's rock classification	Hartmann & Moosdorf (2012) lithology classification
Alluvium	su Unconsolidated sediments + ev Evaporites
Carbonate	sc Carbonate sedimentary rocks
Sand	Siliciclastic sedimentary rocks + sm Mixed sedimentary rocks
Basalt	vb Basic volcanic rocks + pb Basic plutonic rocks + vi Intermediate volcanic rock
Other	va Acid volcanic rocks + m t Metamorphics + pa Acid plutonic rocks + wb Water Bodies + py Pyroclastics + pi Intermediate plutonic rocks + nd No Data + ig Ice and Glaciers

149

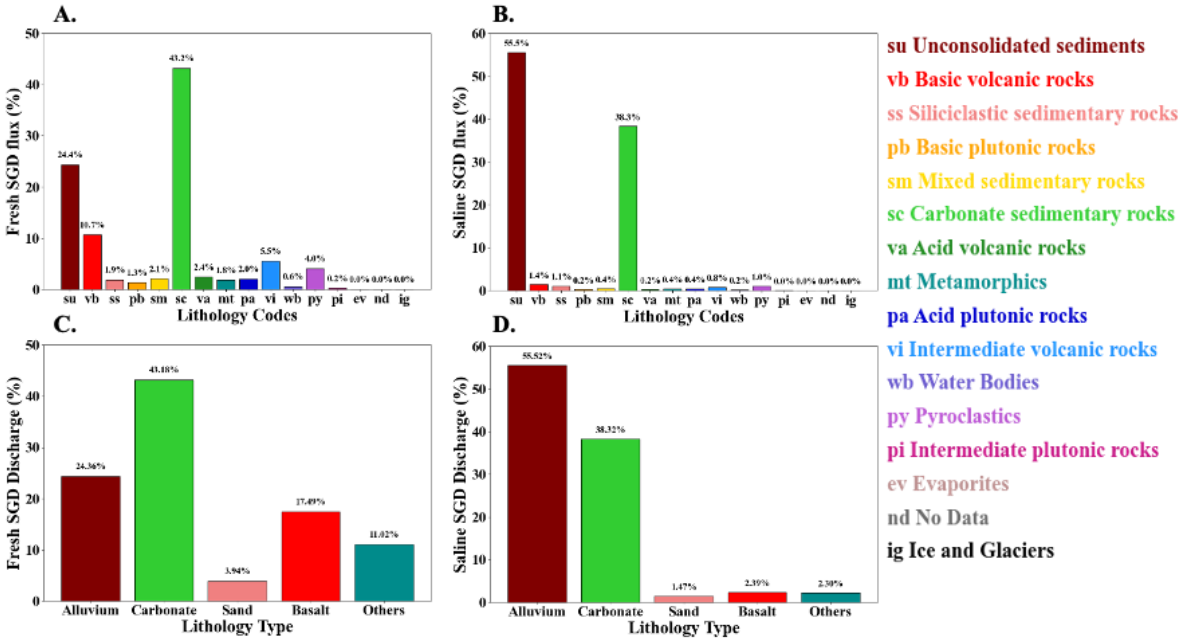

Fig. S1. The discharged percentage by each rock type worldwide for freshwater (61) and the long-term seawater circulation (saline water) are divided into lithological classifications based on high-resolution surface lithology (62) (A for freshwater and B for saline water) as well as our classification (C for freshwater and D for saline water). The colored legend at the right is for the rock classification of subplots A and B.

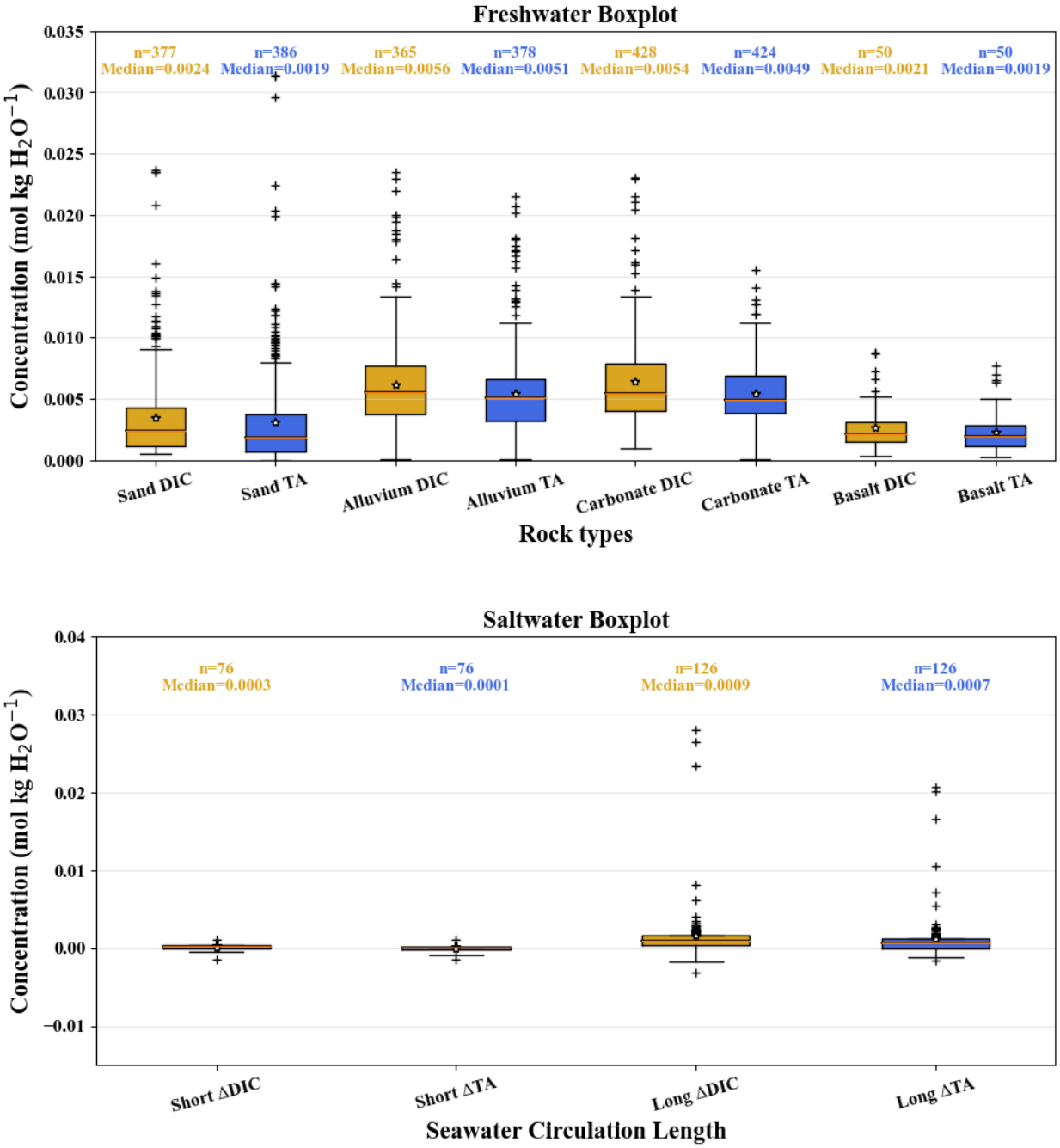

Fig. S2. Boxplots showing concentrations of DIC (brownish-yellow boxes) and TA (blue boxes) in groundwater samples. Upper plot: concentrations across different rock types: Sand, Alluvium, Carbonate, and Basalt in fresh groundwater. Lower plot: concentrations grouped by seawater circulation length (short vs. long) in saline groundwater. In each boxplot, red lines indicate median values and white asterisks denote sample means. Numbers and median concentrations are annotated above each box.

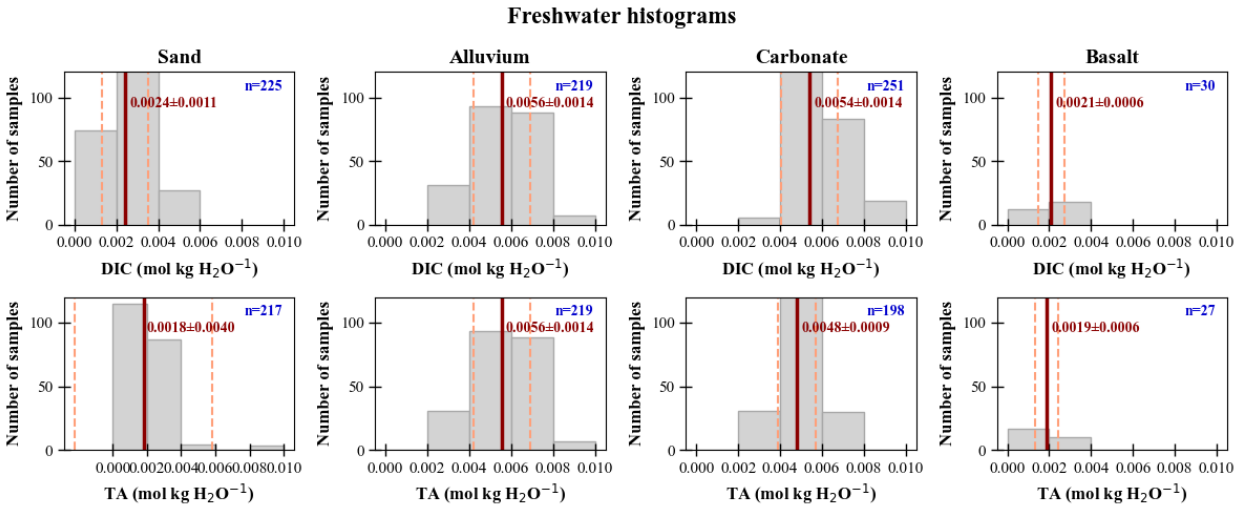

164

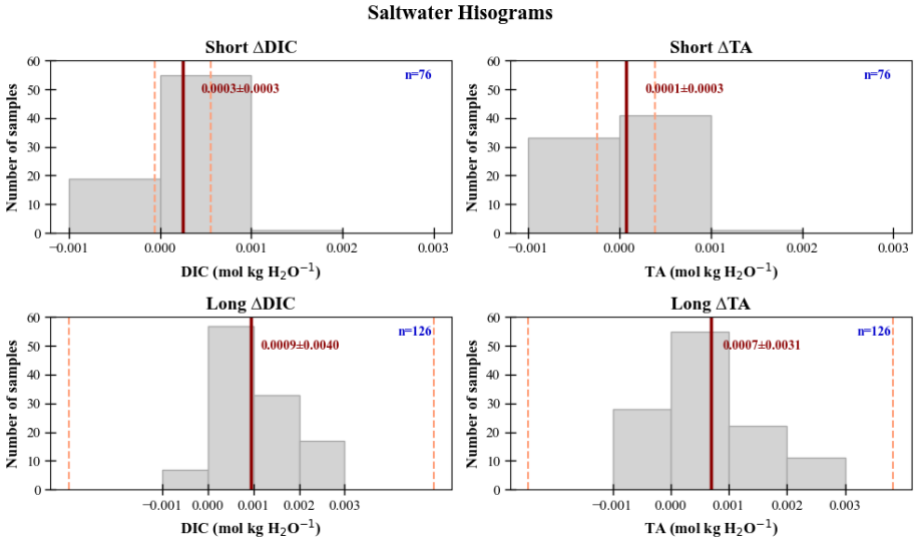

165

166 **Fig. S3**. Histograms showing the distribution of DIC and TA concentrations in groundwater
167 samples. The upper two rows display freshwater samples across different rock types: Sand,
168 Alluvium, Carbonate, and Basalt, based on filtered data from the boxplots in Fig. S2. The lower
169 two rows show saline groundwater samples grouped by short and long seawater circulation
170 lengths. Median values are indicated by red lines, with corresponding values and standard
171 deviations next to them. Dashed red lines represent one standard deviation from the median.
172 Sample sizes (n) are noted in blue in the upper right corner of each subplot.

SI References

1. Parkhurst, D. L. & Appelo, C. A. J. *PHREEQC 2.15. A Computer Program for Speciation, Batch-Reaction, One-Dimentional Transport and Inverse Geochemical Calculation,Water-Resources Investigation*. (1999).
2. Stumm, W. & Morgan, J. J. *Aquatic Chemistry: Chemical Equilibria and Rates in Natural Waters, 3rd Ed.* (John Wiley & Sons, Inc., New York, 1996).
3. Luijendijk, E., Gleeson, T. & Moosdorf, N. Fresh groundwater discharge insignificant for the world's oceans but important for coastal ecosystems. *Nat Commun* **11**, (2020).
4. Hartmann, J. & Moosdorf, N. The new global lithological map database GLiM: A representation of rock properties at the Earth surface. *Geochemistry, Geophysics, Geosystems* **13**, 1–37 (2012).
5. Michael, H. A. *et al.* Geologic influence on groundwater salinity drives large seawater circulation through the continental shelf. *Geophys Res Lett* **43**, 10,782-10,791 (2016).
6. Magaritz, M. & Luzier, J. E. Water-rock interactions and seawater-freshwater mixing effects in the coastal dunes aquifer, Coos Bay, Oregon. *Geochim Cosmochim Acta* **49**, 2515–2525 (1985).
7. Chapelle, F. H., Zelibor, J. L., Grimes, D. J. & Knobel, L. R. L. Bacteria in deep coastal plain sediments of Maryland: A possible source of CO2 to groundwater. *Water Resour Res* **23**, 1625–1632 (1987).
8. Price, R. M. & Herman, J. S. Geochemical investigation of salt-water intrusion into a coastal carbonate aquifer: Mallorca, Spain. *Geol Soc Am Bull* **103**, 1270–1279 (1991).
9. Wicks, M. & Herman, J. S. Regional hydrogeochemistry of a modern coastal mixing zone. *Water Resour Res* **32**, 401–407 (1996).
10. Barker, A. P., Newton, R. J., Bottrell, S. H. & Tellam, J. H. Processes affecting groundwater chemistry in a zone of saline intrusion into an urban sandstone aquifer. *Applied Geochemistry* **13**, 735–749 (1998).
11. Mahlknecht, J., Steinich, B. & Navarro De León, I. Groundwater chemistry and mass transfers in the Independence aquifer, central Mexico, by using multivariate statistics and mass-balance models. *Environmental Geology* **45**, 781–795 (2004).
12. Andersen, M. S., Nyvang, V., Jakobsen, R. & Postma, D. Geochemical processes and solute transport at the seawater/freshwater interface of a sandy aquifer. *Geochim Cosmochim Acta* **69**, 3979–3994 (2005).
13. Charideh, A. & Rahman, A. Environmental isotopic and hydrochemical study of water in the karst aquifer and submarine springs of the Syrian coast. *Hydrogeol J* **15**, 351–364 (2007).
14. Bouchaou, L. *et al.* Application of multiple isotopic and geochemical tracers for investigation of recharge, salinization, and residence time of water in the Souss-Massa aquifer, southwest of Morocco. *J Hydrol (Amst)* **352**, 267–287 (2008).
15. de Montety, V. *et al.* Origin of groundwater salinity and hydrogeochemical processes in a confined coastal aquifer: Case of the Rhône delta (Southern France). *Applied Geochemistry* **23**, 2337–2349 (2008).

16. Gattacceca, J. C. *et al.* Isotopic and geochemical characterization of salinization in the shallow aquifers of a reclaimed subsiding zone: The southern Venice Lagoon coastland. *J Hydrol (Amst)* **378**, 46–61 (2009).
17. Chae, G. T., Yun, S. T., Yun, S. M., Kim, K. H. & So, C. S. Seawater–freshwater mixing and resulting calcite dissolution: an example from a coastal alluvial aquifer in eastern South Korea. *Hydrological Sciences Journal* **57**, 1672–1683 (2012).
18. Vandenbohede, A. & Lebbe, L. Groundwater chemistry patterns in the phreatic aquifer of the central Belgian coastal plain. *Applied Geochemistry* **27**, 22–36 (2012).
19. Ahmed, M. A., Abdel Samie, S. G. & Badawy, H. A. Factors controlling mechanisms of groundwater salinization and hydrogeochemical processes in the Quaternary aquifer of the Eastern Nile Delta, Egypt. *Environ Earth Sci* **68**, 369–394 (2013).
20. Vinson, D. S. *et al.* Occurrence and mobilization of radium in fresh to saline coastal groundwater inferred from geochemical and isotopic tracers (Sr, S, O, H, Ra, Rn). *Applied Geochemistry* **38**, 161–175 (2013).
21. Zhang, W., Chen, X., Tan, H., Zhang, Y. & Cao, J. Geochemical and isotopic data for restricting seawater intrusion and groundwater circulation in a series of typical volcanic islands in the South China Sea. *Mar Pollut Bull* **93**, 153–162 (2015).
22. Díaz-Puga, M. A. *et al.* Groundwater flow and residence time in a karst aquifer using ion and isotope characterization. *International Journal of Environmental Science and Technology* **13**, 2579–2596 (2016).
23. Han, D., Song, X. & Currell, M. J. Identification of anthropogenic and natural inputs of sulfate into a karstic coastal groundwater system in northeast China: Evidence from major ions, δ13 CDIC and δ34SSO4. *Hydrol Earth Syst Sci* **20**, 1983–1999 (2016).
24. Sajil Kumar, P. J. Deciphering the groundwater–saline water interaction in a complex coastal aquifer in South India using statistical and hydrochemical mixing models. *Model Earth Syst Environ* **2**, 1–11 (2016).
25. Santoni, S. *et al.* Residence time, mineralization processes and groundwater origin within a carbonate coastal aquifer with a thick unsaturated zone. *J Hydrol (Amst)* **540**, 50–63 (2016).
26. Carreira, P. M., Bahir, M., Salah, O., Galego Fernandes, P. & Nunes, D. Tracing salinization processes in coastal aquifers using an isotopic and geochemical approach: comparative studies in western Morocco and southwest Portugal. *Hydrogeol J* **26**, 2595–2615 (2018).
27. Han, D. & Currell, M. J. Delineating multiple salinization processes in a coastal plain aquifer, northern China: Hydrochemical and isotopic evidence. *Hydrol Earth Syst Sci* **22**, 3473–3491 (2018).
28. Vallejos, A., Sola, F., Yechieli, Y. & Pulido-Bosch, A. Influence of the paleogeographic evolution on the groundwater salinity in a coastal aquifer. Cabo de Gata aquifer, SE Spain. *J Hydrol (Amst)* **557**, 55–66 (2018).
29. Mohanty, A. K. & Rao, V. V. S. G. Hydrogeochemical, seawater intrusion and oxygen isotope studies on a coastal region in the Puri District of Odisha, India. *Catena (Amst)* **172**, 558–571 (2019).
30. Monnin, C. *et al.* Freshening of a Coastal Karst Aquifer Revealed by the Temporal Changes in a Spring Water Composition (La Palme, Southern France). *Hydrology* **2**, 45 (2019).

31. Naus, F. L., Schot, P., Groen, K., Matin Ahmed, K. & Griffioen, J. Groundwater salinity variation in Upazila Assasuni (southwestern Bangladesh), as steered by surface clay layer thickness, relative elevation and present-day land use. *Hydrol Earth Syst Sci* **23**, 1431–1451 (2019).
32. Yechieli, Y. *et al.* Recent seawater intrusion into deep aquifer determined by the radioactive noble-gas isotopes 81Kr and 39Ar. *Earth Planet Sci Lett* **507**, 21–29 (2019).
33. Houéménou, H. *et al.* Degradation of groundwater quality in expanding cities in West Africa. A case study of the unregulated shallow aquifer in Cotonou. *J Hydrol (Amst)* **582**, (2020).
34. Okuhata, B. K., Dulai, H., Shuler, C. K., Fackrell, J. K. & El-Kadi, A. I. Metal mobilization as an effect of anthropogenic contamination in groundwater aquifers in Tutuila, American samoa. *Water (Switzerland)* **12**, (2020).
35. Pain, A. J., Martin, J. B., Young, C. R., Valle-Levinson, A. & Mariño-Tapia, I. Carbon and phosphorus processing in a carbonate karst aquifer and delivery to the coastal ocean. *Geochim Cosmochim Acta* **269**, 484–495 (2020).
36. Vallejos, A., Daniele, L., Sola, F., Molina, L. & Pulido-Bosch, A. Anthropic-induced salinization in a dolomite coastal aquifer. Hydrogeochemical processes. *J Geochem Explor* **209**, (2020).
37. Godfrey, L. V. *et al.* δ13C and 14C activity of groundwater DOC and DIC in the volcanically active and arid Loa Basin of northern Chile. *J Hydrol (Amst)* **595**, (2021).
38. Zhang, B. & Zhang, J. The hydrological connection between fresh submarine groundwater discharge and coastal groundwater: an isotopic and a decadal hydrochemistry approach in an alluvial fan, central Japan. *Environ Earth Sci* **80**, (2021).
39. Sola, F. & Vallejos, A. Long and short-term cation exchange linked to a negative hydraulic barrier in a coastal aquifer. *Science of the Total Environment* **819**, (2022).
40. Cai, W. J., Wang, Y., Krest, J. & Moore, W. S. The geochemistry of dissolved inorganic carbon in a surficial groundwater aquifer in North Inlet, South Carolina, and the Carbon fluxes to the coastal ocean. *Geochim Cosmochim Acta* **67**, 631–639 (2003).
41. Gramling, C. M., McCorkle, D. C., Mulligan, A. E. & Woods, T. L. A carbon isotope method to quantify groundwater discharge at the land-sea interface. *Limnol Oceanogr* **48**, 957–970 (2003).
42. Sivan, O., Yechieli, Y., Herut, B. & Lazar, B. Geochemical evolution and timescale of seawater intrusion into the coastal aquifer of Israel. *Geochim Cosmochim Acta* **69**, 579–592 (2005).
43. Russak, A. & Sivan, O. Hydrogeochemical tool to identify salinization or freshening of coastal aquifers determined from combined field work, experiments, and modeling. *Environ Sci Technol* **44**, 4096–4102 (2010).
44. Bakari, S. S. *et al.* Groundwater residence time and paleorecharge conditions in the deep confined aquifers of the coastal watershed, South-East Tanzania. *J Hydrol (Amst)* **466–467**, 127–140 (2012).

45. Liu, Q. *et al.* How significant is submarine groundwater discharge and its associated dissolved inorganic carbon in a river-dominated shelf system? *Biogeosciences* **9**, 1777–1795 (2012).
46. Liu, Q. *et al.* Effect of submarine groundwater discharge on the coastal ocean inorganic carbon cycle. *Limnol Oceanogr* **59**, 1529–1554 (2014).
47. Wang, G. *et al.* Coastal acidification induced by tidal-driven submarine groundwater discharge in a coastal coral reef system. *Environ Sci Technol* **48**, 13069–13075 (2014).
48. Lee, J. & Kim, G. Dependence of coastal water pH increases on submarine groundwater discharge off a volcanic island. *Estuar Coast Shelf Sci* **163**, 15–21 (2015).
49. Wang, G. *et al.* Net subterranean estuarine export fluxes of dissolved inorganic C, N, P, Si, and total alkalinity into the Jiulong River estuary, China. *Geochim Cosmochim Acta* **149**, 103–114 (2015).
50. Sadat-Noori, M., Maher, D. T. & Santos, I. R. Groundwater Discharge as a Source of Dissolved Carbon and Greenhouse Gases in a Subtropical Estuary. *Estuaries and Coasts* **39**, 639–656 (2016).
51. Bryan, E., Meredith, K. T., Baker, A., Andersen, M. S. & Post, V. E. A. Carbon dynamics in a Late Quaternary-age coastal limestone aquifer system undergoing saltwater intrusion. *Science of the Total Environment* **607–608**, 771–785 (2017).
52. Caschetto, M., Colombani, N., Mastrocicco, M., Petitta, M. & Aravena, R. Nitrogen and sulphur cycling in the saline coastal aquifer of Ferrara, Italy. A multi-isotope approach. *Applied Geochemistry* **76**, 88–98 (2017).
53. Liu, Q. *et al.* Carbonate system biogeochemistry in a subterranean estuary – Waquoit Bay, USA. *Geochim Cosmochim Acta* **203**, 422–439 (2017).
54. Prouty, N. G. *et al.* Vulnerability of Coral Reefs to Bioerosion From Land-Based Sources of Pollution. *J Geophys Res Oceans* **122**, 9319–9331 (2017).
55. Bandara, U. G. C. *et al.* Arsenic-rich shallow groundwater in sandy aquifer systems buffered by rising carbonate waters: A geochemical case study from Mannar Island, Sri Lanka. *Science of the Total Environment* **633**, 1352–1359 (2018).
56. Meredith, K. T. *et al.* Evolution of dissolved inorganic carbon in groundwater recharged by cyclones and groundwater age estimations using the 14C statistical approach. *Geochim Cosmochim Acta* **220**, 483–498 (2018).
57. Murgulet, D. *et al.* Temporal and spatial fluctuations of groundwater-derived alkalinity fluxes to a semiarid coastal embayment. *Science of the Total Environment* **630**, 1343–1359 (2018).
58. Tan, E., Wang, G., Moore, W. S., Li, Q. & Dai, M. Shelf-Scale Submarine Groundwater Discharge in the Northern South China Sea and East China Sea and its Geochemical Impacts. *J Geophys Res Oceans* **123**, 2997–3013 (2018).
59. Dai, G., Wang, G., Li, Q., Tan, E. & Dai, M. Submarine Groundwater Discharge on the Western Shelf of the Northern South China Sea Influenced by the Pearl River Plume and Upwelling. *J Geophys Res Oceans* **126**, (2021).

60. Kolker, D., Bookman, R., Herut, B., David, N. & Silverman, J. An Initial Assessment of the Contribution of Fresh Submarine Ground Water Discharge to the Alkalinity Budget of the Mediterranean Sea. *J Geophys Res Oceans* **126**, 1–10 (2021).
61. Liu, Y. *et al.* Inorganic carbon and alkalinity biogeochemistry and fluxes in an intertidal beach aquifer: Implications for ocean acidification. *J Hydrol (Amst)* **595**, 126036 (2021).
62. Reithmaier, G. M. S. *et al.* Rainfall drives rapid shifts in carbon and nutrient source-sink dynamics of an urbanised, mangrove-fringed estuary. *Estuar Coast Shelf Sci* **249**, (2021).